Similar results were obtained for a reaction mixture prepared by treating 0.17 g of polymer IIB with 0.025 g of $Co_2(CO)_8$ at 180 °C. In both cases the IR spectra were nearly identical: IR (THF, ν(CO) (cm^{-1})) 2045 (w), 2020 (sh), 1998 (s), 1970 (vw), 1935 (m), 1885 (vs).

(7) Hydroformylation of 1-Hexene. Polymers. The following reaction conditions were used in all of the catalytic runs involving the polymers. $Co_2(CO)_8$ (0.04 g) was placed in 20 mL of THF, and the polymer (0.04 g) was added. 1-Hexene (4.0 g) and 1.0 g of *n*-decane were added, causing the homogeneous catalyst to precipitate. The reaction mixture was placed in a stirring autoclave, purged twice with argon, and then pressurized to 1500 psig of CO and H_2 (1:2). The reactor was heated to 190 °C, and the mixture was stirred for 10 h and then slowly cooled. The homogeneous red solution was sampled for GLC analysis. See Table I for GLC results.

Oligomers. $Co_2(CO)_8$ (0.04 g) was dissolved in 20 mL of toluene. The appropriate amount of oligomer then was added. 1-Hexene (4.0 g) and 1.0 g of *n*-decane were added, and the reaction mixture was placed in a stirring autoclave, flushed with argon, and pressurized to 1500 psig of CO and H_2 (1:2). The reactor was heated to 170 °C and kept at that temperature for 3 h. The homogeneous red solution was sampled for GLC analysis. See Table I for GLC results.

Acknowledgment. Thanks to Dr. C. W. Jung, Dr. L. Messerle, Prof. G. L. Geoffroy, Prof. K. G. Caulton, and Prof. H. H. Karsch for helpful discussions on the complex NMR spectra of these systems. Some of the NMR measurements were made at Yale University NSF Northeast Regional NMR Facility funded under NSF Grant CHE-791620. The work carried out at the Massachusetts Institute of Technology was supported by the National Science Foundation and by a Dow Chemical Co. fellowship to H.P.W.

Registry No. I (x = 1), 12098-17-8; I (x = 2), 82311-92-0; I (x = 3), 82311-93-1; I (x = 4), 82322-77-8; III (x = 1), 12150-46-8; III (x = 2), 82311-96-4; IV, 85267-29-4; Va, 85250-09-5; Vb, 85250-11-9; VI, 85250-13-1; VII, 85250-16-4; VIII, 85250-19-7; $[Co(CO)_3(PPh_2Fc)]_2$, 85250-07-3; $[Co(CO)_2(L \sim L' \sim L)][BPh_4]$, 85250-14-2; $[Co(CO)_2(L'' \sim L' \sim L)][BPh_4]$, 85250-17-5; $[Co(CO)_2(L''' \sim L'' \sim L' \sim L)][BPh_4]$, 85250-20-0; $Co_2(CO)_8$, 10210-68-1; 1-hexene, 592-41-6.

Crystal, Geometrical, and Electronic Structure of $HFe_4(CO)_{12}BH_2$. A Boron Analogue of a Protonated Carbido Cluster

T. P. Fehlner,* C. E. Housecroft, W. R. Scheidt, and K. S. Wong

Department of Chemistry, University of Notre Dame, Notre Dame, Indiana 46556

Received November 22, 1982

The new ferraborane $HFe_4(CO)_{12}BH_2$ has been prepared and structurally characterized by a single-crystal, X-ray diffraction study. This compound, which is a $HFe_4(CO)_{12}$ "butterfly" fragment with a BH_2 fragment bridging the "wing-tips", is isoelectronic as well as structurally related to $HFe_4(CO)_{12}CH$ an iron cluster containing a Fe–H–C interaction. The geometrical and electronic structure of this ferraborane is analyzed in terms of electron-counting rules as well as with a fragment analysis utilizing the Fenske–Hall approach. This analysis demonstrates that the ferraborane is most properly described either as an arachno, four-atom cluster with an interstitial boron atom or as a saturated, 62-electron complex with the BH_2 ligand contributing five electrons. The orientation of the BH_2 fragment with respect to the iron butterfly is explained in terms of the special properties of the frontier orbitals of the tetrametal fragment. The interaction of a filled cluster orbital with an empty B–H antibonding orbital of free BH_2 provides a logical explanation for the strong Fe–H–B three-center interaction in $HFe_4(CO)_{12}BH_2$ and a justification for considering the ferraborane a hydrogenated iron boride cluster. Crystals of $HFe_4(CO)_{12}BH_2$ form in the monoclinic space group $P2_1/c$ with the following unit-cell parameters: a = 16.429 (5) Å, b = 8.740 (3) Å, c = 13.237 (3) Å, β = 94.32 (1)°, V = 1896 Å^3, Z = 4. The X-ray structure was solved as described in the text and refined to R_1 = 0.044 and R_2 = 0.045 for 2817 independent reflections.

In the past few years there has been a substantial number of homonuclear four-metal cluster compounds in which the metal atoms are arranged in a so-called "butterfly" array (Figure 1a) reported.[1-7] Usually in these compounds there is an atom or group of atoms (X) bridging the "wing-tip" metals; however, recently an example of an unsupported osmium butterfly complex was reported.[8] The structural parameters of a variety of tetrairon complexes have been compared previously,[1] and it appears that the two most sensitive to variation in X are the dihedral

(1) Tachikawa, M.; Muetterties, E. L. *J. Am. Chem. Soc.* **1980**, *102*, 4541. Beno, M. A.; William, J. M.; Tachikawa, M.; Muetterties, E. L. *Ibid.* **1980**, *102*, 4542. Beno, M. A.; Williams, J. M.; Tachikawa, M.; Muetterties, E. L. *Ibid.* **1981**, *103*, 1485.

(2) Whitmire, K. H.; Shriver, D. F. *J. Am. Chem. Soc.* **1981**, *103*, 6754. Holt, E. M.; Whitmire, K. H.; Shriver, D. F. *J. Organomet. Chem.* **1981**, *213*, 125.

(3) Bradley, J. S.; Ansell, G. B.; Hill, E. W. *J. Am. Chem. Soc.* **1979**, *101*, 7418. Bradley, J. S.; Ansell, G. B.; Leonowicz, M. E.; Hill, E. W. *Ibid.* **1981**, *103*, 4968.

(4) Fjare, D. E.; Gladfelter, W. L. *Inorg. Chem.* **1981**, *20*, 3532.

(5) Manassero, M.; Sansoni, M.; Longoni, G. *J. Chem. Soc., Chem. Commun.* **1976**, 919.

(6) Wong, K. W.; Scheidt, W. R.; Fehlner, T. P. *J. Am. Chem. Soc.* **1982**, *104*, 1111.

(7) Carty, A. J.; MacLaughlin, S. A.; Van Wagner, J.; Taylor, N. *Organometallics* **1982**, *1*, 1013.

(8) Johnson, B. F. G.; Lewis, J.; Nelson, W. J. H.; Puga, J.; Raithby, P. R.; Shröeder, M.; Whitmire, K. H. *J. Chem. Soc., Chem. Commun.* **1982**, 610.

0276-7333/83/2302-0825$01.50/0

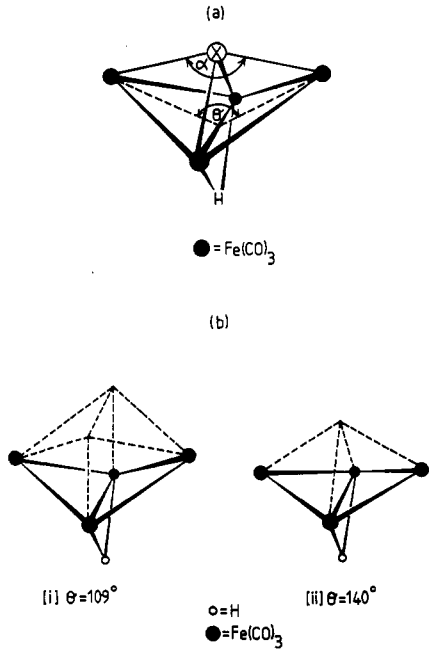

Figure 1. (a) Schematic drawing of a tetrametal complex having a "butterfly" geometry with a ligand X bridging the wing-tip metal atoms. The angles θ (dihedral angle) and α define parameters sensitive to electronic structure. (b) The ideal dihedral angles of the butterfly fragment for a four-atom arachno cluster and a five-atom nido structure. X is considered interstitial in (i) and skeletal in (ii).

angle (θ) and the M–X–M angle (α) between bridging X group and wing-tip metals (Figure 1). The butterfly tetrametal fragment is clearly an important one in that it serves to bind various organic and inorganic fragments in unusual ways, e.g., side on bound CH[1] and CO[5] as well as bare carbon[3] and nitrogen atoms.[4]

We have prepared a member of the butterfly iron series containing a BH_2 fragment bridging the wing-tip metal atoms.[6] This compound, $HFe_4(CO)_{12}BH_2$ (I), is isoelectronic with $HFe_4(CO)_{12}CH$.[1] Herein we present the complete structural details of this compound. In addition we present a detailed analysis of the bonding in $HFe_4(CO)_{12}BH_2$ using the Fenske–Hall nonparameterized quantum chemical technique.[9] In doing so we evaluate the bonding capabilities of the tetrairon butterfly fragment and give a description of the electronic structures of $HFe_4(CO)_{12}X$ where X = BH_2, BH^-, and CH_2^+. These results as well as the intercomparison of appropriately chosen calculated electron density contour diagrams are used to argue that I contains a BH_2 ligand in which the BH bonds have been substantially weakened.

Experimental Section

Preparation of I. Reactions were carried out under an atmosphere of nitrogen or with standard vacuum line techniques. In pentane (~1.5 mL) $B_2H_6Fe_2(CO)_6$[10] (~0.2 mmol) and an excess amount of $Fe_2(CO)_9$ were allowed to react at 25 °C for 7 h. The color of the mixture changed from light orange to greenish brown. After the removal of solvent and more volatile starting material, the two products were separated by sublimation, the major and least volatile product, I, being a very dark brown solid, soluble in hydrocarbons and somewhat air sensitive.

X-ray Crystallographic Data. Crystals suitable for an X-ray diffraction study were grown from a polycrystalline sample at 45–50 °C in an evacuated capillary. A single crystal, 0.3 × 0.2 × 0.15 mm^3, was chosen for analysis. The crystal was found to be monoclinic, with cell dimensions a = 16.429 (5) Å, b = 8.740 (3) Å, c = 13.237 (3) Å, β = 94.32 (1)°, and V = 1896 Å^3. The space group was determined as $P2_1/c$ with Z = 4 and a calculated density of 2.01 g cm^{-3}. Diffraction data were collected at 293 K on a Syntex P$\bar{1}$ diffractometer, using graphite-monochromated Mo Kα radiation. One octant of data was collected by the θ–2θ scan technique, with scan speeds varying from 2 to 12°/min, to the limit 2θ < 55°. The intensities of four standard reflections, monitored at regular intervals, showed no significant fluctuation during the collection procedure. The raw intensity data were corrected for Lorentz and polarization effects. No absorption correction has been applied [μ(Mo Kα) = 30.6 cm^{-1}]. After equivalent reflections were averaged, a total of 2817 independent reflections were used for solution and refinement.

Solution and Refinement of the Structure. The iron atoms were located by direct methods with use of the MULTAN[11] package. The rest of the atoms were located by Fourier techniques. Full-matrix least-squares refinement was based on minimization of the function $\sum\omega(|F_o| - |F_c|)^2$,[11] where F_o and F_c are the observed and calculated structure factor amplitudes, respectively. Atomic scattering factors for non-hydrogen atoms were taken from Cromer and Weber.[12] All hydrogen atoms were refined isotropically, and all other atoms were refined anisotropically. The final conventional residual was R_1 = 0.044 and the weighted residual, $R_2 = [\sum\omega(|F_o| - |F_c|)^2/\sum\omega|F_o|^2]^{1/2}$ = 0.045. The final difference Fourier synthesis displayed a background density of 0.2–0.3 e Å^{-3} throughout the unit cell. The estimated standard deviation of an observation of unit weight is 1.22. Atomic coordinates for all atoms are listed in Table I. Interatomic

Table I. Final Positional Parameters for $HFe_4(BH_2)(CO)_{12}$[a]

atom	x	y	z
Fe_1	0.78352 (4)	0.41457 (7)	0.77204 (5)
Fe_2	0.85313 (4)	0.58834 (8)	0.63718 (5)
Fe_3	0.73620 (4)	0.70105 (8)	0.74568 (5)
Fe_4	0.63242 (4)	0.47369 (9)	0.69502 (6)
O_{11}	0.9439 (2)	0.3844 (5)	0.8843 (3)
O_{12}	0.8032 (3)	0.1480 (4)	0.6433 (3)
O_{13}	0.7117 (3)	0.2366 (6)	0.9296 (3)
O_{21}	0.8777 (2)	0.8549 (5)	0.5095 (3)
O_{22}	0.9909 (3)	0.6732 (6)	0.7784 (3)
O_{23}	0.9486 (3)	0.3645 (5)	0.5332 (4)
O_{31}	0.6173 (3)	0.8234 (5)	0.8789 (4)
O_{32}	0.8563 (3)	0.9246 (5)	0.8284 (3)
O_{33}	0.6758 (3)	0.8828 (4)	0.5715 (3)
O_{41}	0.5663 (2)	0.4721 (5)	0.8949 (3)
O_{42}	0.5825 (3)	0.1563 (5)	0.6554 (5)
O_{43}	0.4924 (3)	0.6336 (6)	0.5943 (4)
C_{11}	0.8828 (3)	0.4001 (6)	0.8392 (4)
C_{12}	0.7957 (3)	0.2517 (6)	0.6937 (4)
C_{13}	0.7365 (3)	0.3117 (7)	0.8687 (4)
C_{21}	0.8687 (3)	0.7521 (6)	0.5592 (4)
C_{22}	0.9355 (3)	0.6397 (7)	0.7255 (4)
C_{23}	0.9124 (3)	0.4509 (7)	0.5752 (4)
C_{31}	0.6628 (4)	0.7686 (6)	0.8269 (4)
C_{32}	0.8125 (4)	0.8350 (6)	0.7952 (4)
C_{33}	0.6993 (3)	0.8129 (6)	0.6399 (4)
C_{41}	0.5932 (3)	0.4752 (6)	0.8184 (5)
C_{42}	0.6006 (3)	0.2798 (7)	0.6699 (5)
C_{43}	0.5462 (3)	0.5742 (7)	0.6346 (4)
B	0.7387 (3)	0.5254 (6)	0.6436 (4)
H_{13}	0.7742 (26)	0.5719 (50)	0.8352 (33)
H_{2B}	0.7824 (31)	0.5364 (61)	0.5610 (39)
H_{4B}	0.6693 (32)	0.4734 (63)	0.5883 (40)

[a] The estimated standard deviations of the least significant digits are given in parentheses.

(9) Hall, M. B.; Fenske, R. F. *Inorg. Chem.* **1972**, *11*, 768. Hall, M. B. Ph.D. Thesis, University of Wisconsin, Madison, WI, 1971. Fenske, R. F. *Pure Appl. Chem.* **1971**, *27*, 61.

(10) Andersen, E. L.; Fehlner, T. P. *J. Am. Chem. Soc.* **1978**, *100*, 4606.

(11) Germain, G.; Main, P.; Woolfson, M. M. *Acta Crystallogr., Sect. A* **1971**, *A27*, 368. Other programs used as well as a description of data collection and data reduction methods can be found in: Scheidt, W. R. *J. Am. Chem. Soc.* **1974**, *96*, 84.

(12) Cromer, D. T.; Weber, J. T. "International Tables for X-ray Crystallography"; Kynoch Press: Birmingham, England, 1974; Vol. 4.

Table II. Interatomic Distances (Å) for $HFe_4(BH_2)(CO)_{12}$ [a]

Fe_1-Fe_2	2.666 (1)	Fe_2-C_{23}	1.784 (6)
Fe_2-Fe_3	2.672 (1)	Fe_3-C_{31}	1.776 (7)
Fe_3-Fe_4	2.671 (1)	Fe_3-C_{32}	1.803 (6)
Fe_1-Fe_3	2.637 (1)	Fe_3-C_{33}	1.776 (6)
Fe_1-Fe_4	2.662 (1)	Fe_4-C_{41}	1.801 (7)
B-Fe_1	2.044 (6)	Fe_4-C_{42}	1.797 (7)
B-Fe_3	2.047 (6)	Fe_4-C_{43}	1.794 (7)
B-Fe_2	1.966 (6)	C_{11}-O_{11}	1.137 (6)
B-Fe_4	1.974 (6)	C_{12}-O_{12}	1.137 (6)
H_{13}-Fe_1	1.62 (4)	C_{13}-O_{13}	1.138 (6)
H_{13}-Fe_3	1.72 (4)	C_{21}-O_{21}	1.130 (6)
H_{2b}-B	1.36 (5)	C_{22}-O_{22}	1.144 (6)
H_{2b}-Fe_2	1.55 (5)	C_{23}-O_{23}	1.134 (7)
H_{4b}-B	1.38 (5)	C_{31}-O_{31}	1.158 (7)
H_{4b}-Fe_4	1.58 (5)	C_{32}-O_{32}	1.130 (6)
Fe_1-C_{11}	1.803 (6)	C_{33}-O_{33}	1.136 (6)
Fe_1-C_{12}	1.781 (6)	C_{41}-O_{41}	1.135 (7)
Fe_1-C_{13}	1.787 (6)	C_{42}-O_{42}	1.132 (7)
Fe_2-C_{21}	1.794 (6)	C_{43}-O_{43}	1.132 (7)
Fe_2-C_{22}	1.779 (6)		

[a] Numbers in parentheses are estimated standard deviations.

Table III. Selected Bond Angles (deg) for $HFe_4(BH_2)(CO)_{12}$ [a]

Fe_1-B-Fe_3	80.3 (2)	C_{42}-Fe_4-C_{43}	99.3 (3)
Fe_1-Fe_2-Fe_3	59.20 (3)	Fe_1-C_{11}-O_{11}	176.3 (5)
Fe_1-Fe_4-Fe_3	59.28 (3)	Fe_1-C_{12}-O_{12}	179.6 (5)
B-H_{2b}-Fe_2	85.0 (28)	Fe_1-C_{13}-O_{13}	173.9 (5)
Fe_2-Fe_1-Fe_3	60.51 (3)	Fe_2-C_{21}-O_{21}	179.3 (5)
B-H_{4b}-Fe_4	83.3 (28)	Fe_2-C_{22}-O_{22}	176.7 (5)
Fe_4-Fe_3-Fe_1	60.20 (3)	Fe_2-C_{23}-O_{23}	177.9 (6)
Fe_1-H_{13}-Fe_3	104.2 (23)	Fe_3-C_{31}-O_{31}	174.9 (6)
Fe_2-B-Fe_3	83.5 (2)	Fe_3-C_{32}-O_{32}	175.5 (6)
Fe_1-B-Fe_4	82.9 (2)	Fe_3-C_{33}-O_{33}	179.1 (5)
Fe_4-B-Fe_3	83.2 (2)	Fe_4-C_{41}-O_{41}	177.4 (6)
H_{2b}-B-H_{4b}	93.5 (30)	Fe_4-C_{42}-O_{42}	178.1 (6)
H_{2b}-Fe_2-B	43.4 (18)	Fe_4-C_{43}-O_{43}	178.3 (6)
H_{4b}-Fe_4-B	44.1 (19)	Fe_1-Fe_2-C_{21}	157.9 (2)
H_{13}-Fe_1-B	89.1 (15)	Fe_1-Fe_2-C_{22}	92.7 (2)
C_{11}-Fe_1-C_{12}	95.4 (2)	Fe_1-Fe_2-C_{23}	101.6 (2)
C_{12}-Fe_1-C_{13}	95.1 (3)	Fe_3-Fe_2-C_{21}	98.9 (2)
C_{11}-Fe_1-C_{13}	92.0 (2)	Fe_3-Fe_2-C_{22}	95.5 (2)
C_{21}-Fe_2-C_{22}	92.4 (2)	Fe_3-Fe_2-C_{23}	159.2 (2)
C_{22}-Fe_2-C_{23}	93.3 (3)	Fe_2-Fe_3-C_{31}	175.2 (2)
C_{21}-Fe_2-C_{23}	99.6 (3)	Fe_2-Fe_3-C_{32}	85.8 (2)
C_{31}-Fe_3-C_{32}	92.8 (3)	Fe_2-Fe_3-C_{33}	89.8 (2)
C_{31}-Fe_3-C_{33}	94.9 (3)	Fe_4-Fe_3-C_{31}	87.1 (2)
C_{32}-Fe_3-C_{33}	96.7 (2)	Fe_4-Fe_3-C_{32}	171.1 (2)
C_{41}-Fe_4-C_{42}	93.2 (3)	Fe_4-Fe_3-C_{33}	92.2 (2)
C_{41}-Fe_4-C_{43}	94.3 (3)		

[a] Numbers in parentheses are estimated standard deviations.

distances and intramolecular angles are listed in Tables II and III, respectively.

Calculations. Fenske–Hall calculations were carried out on the three complexes $HFe_4(CO)_{12}X$ where X = BH_2, BH^-, and CH_2^+. The geometries of the ferraborane complexes were taken from the X-ray structural study reported herein. For $HFe_4(CO)_{12}CH_2^+$ the iron butterfly was taken from the structure of $HFe_4(CO)_{12}BH_2$ and the ligand position, CH distance, and HCH angle were based on the known structure of $HFe_4(CO)_{12}CH$.[1] It should be noted that the resulting HCH angle, 66°, is somewhat unrealistic. In all cases the geometry of the butterfly fragment was idealized to C_{2v} symmetry and all C–O bond lengths were set at 1.13 Å and Fe–CO bond lengths at 1.80 Å. The calculations employed single-ζ Slater basis functions for the 1s and 2s functions of B, C, and O. The exponents were obtained by curve fitting the double-ζ functions of Clementi[13] while orthogonal functions were maintained; the double-ζ functions were used directly for the 2p orbitals. For hydrogen, an exponent of 1.16 was used. The iron 1s-3d functions were taken from the results of Richardson et al.[14] and were all single-ζ except the 3d function, which is double-ζ and was chosen for the +1 oxidation state. Both the 4s and the 4p exponents were chosen to be 2.0.

(13) Clementi, E. *J. Chem. Phys.* **1964**, *40*, 1944.

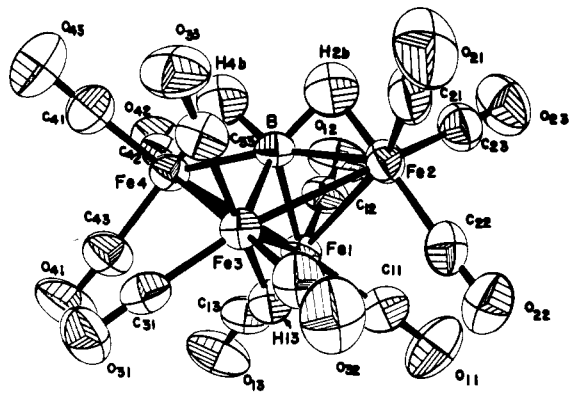

Figure 2. An ORTEP drawing of the structure of $HFe_4(CO)_{12}BH_2$ (I). The atoms, including hydrogen, are represented at 50% thermal elipsoids.

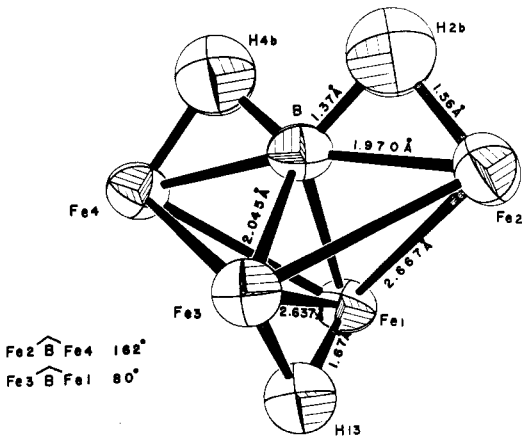

Figure 3. View of the cluster core of $HFe_4(CO)_{12}BH_2$ showing significant interatomic distances.

Description of the Molecular Structure

The ORTEP drawing of $HFe_4(CO)_{12}BH_2$ is shown in Figure 2. The atoms, including hydrogens, are represented at 50% thermal elipsoids. Another drawing of I with the carbonyl groups omitted to reveal the cluster geometry more clearly is shown in Figure 3. The molecule, I, contains a typical butterfly array of four iron atoms, each with three terminal carbonyl ligands. The boron atom is nearly centered between the wing-tips of the Fe_4 array with the bridging hydrogens located between the boron and wing-tip Fe atoms. The Fe(4)–B–Fe(2) angle is 162°, and the boron lies ~0.3 Å from the line joining the wing-tip iron atoms.

First, brief comparison to known Fe_4C butterfly structures[1-5] is worthwhile. The average Fe–Fe edge distance in I of 2.667 (1) Å and the H-bridged Fe–Fe distance of 2.637 (1) Å are similar to those found in other "saturated" Fe_4C complexes.[1-5] All 12 carbonyl ligands are terminally bound, three to each iron atom. The average Fe–C distance is 1.788 (6) Å, and the C–O distance is 1.137 (6) Å. Regarding the iron–boron skeletal distances in I, the pair Fe(2)–B and Fe(4)–B averages to 1.970 (6) Å and the other pair Fe(1)–B and Fe(3)–B to 2.045 (6) Å. The dihedral angle defined by the Fe(4)–Fe(3)–Fe(1) and Fe(3)–Fe-

(14) Richardson, J. W.; Nieuwpoort, W. C.; Powell, R. R.; Edgell, W. F. *J. Chem. Phys.* **1962**, *36*, 1057.

Table IV. Mean Planes and Dihedral Angles of Carbonyl Oxygen Atoms

atom	dist to plane, Å	atom	dist to plane, Å
Plane 1. O_{11}, O_{13}, O_{41}, O_{31}, O_{32}, O_{22}			
$-0.1454x - 0.1780y - 0.9732z = -13.7736$			
O_{11}	0.311	O_{31}	0.146
O_{13}	0.102	O_{32}	0.232
O_{41}	−0.319	O_{22}	−0.472
Plane 2. O_{23}, O_{12}, O_{42}, O_{43}, O_{33}, O_{21}			
$-0.1536x - 0.1841y - 0.9708z = -10.0595$			
O_{23}	−0.328	O_{43}	−0.272
O_{12}	0.351	O_{33}	0.304
O_{42}	−0.039	O_{21}	−0.016
Dihedral Angle between Planes: 0.6°			

(1)–Fe(2) planes is 114°, which is similar to that found in the isoelectronic $HFe_4(CO)_{12}CH$ cluster.[1] Despite the presence of a bridging hydrogen, the Fe(1)–Fe(3) distance is not much different from the other Fe–Fe separations (see Table III).

The spatial arrangement of the terminal carbonyl groups, while appearing to minimize nonbonded interactions, also exhibits an interesting feature. There are two sets of carbonyl oxygen atoms. Each set has six roughly coplanar atoms and the planes in which the atoms lie are parallel (see Table IV). The oxygens thereby form a crude hexagonal antiprism. If one assumes that I is formed from the insertion of a BH_2 group into an edge of a hypothetical tetrahedral $Fe_4(CO)_{12}$, the degree of opening, which depends on the group inserted between wing-tip atoms determines the outward bending of the wing-tip $Fe(CO)_3$ groups. This results in the symmetrical, but fortuitous, arrangement of the carbonyl oxygen atoms observed here.

The sturctural parameters associated with the BH_2 group are of particular interest. The average Fe–H and B–H distances are similar to those found in another iron–boron cluster compound, $B_3H_7Fe_2(CO)_6$,[15] containing Fe–H–B interactions (1.56 (5) and 1.37 (5) Å for I vs. 1.61 (4) and 1.32 (4) Å). The Fe–H distance also agrees well with those found in $B_5H_8Fe(CO)_3^-$ and $(CO)_3FeB_5H_8Cu(PPh_3)_2$.[16] The average wing-tip iron–boron distance in I (1.970 (6) Å) is considerably shorter than the equivalent Fe–B distance in $B_3H_7Fe_2(CO)_6$ (2.263 (4) Å), thereby unambiguously demonstrating that I contains a direct iron–boron interaction; i.e., the Fe–H–B interaction is of the closed three-center type. By implication the structural parameters of I support our previous interpretation[15] of the Fe–H–B interaction in $B_3H_7Fe_2(CO)_6$ as being of the open three-center type.

As $HFe_4(CO)_{12}CH$ is isoelectronic with I and contains a Fe–H–C interaction, a comparison of structural parameters is of interest despite the fact that the location of the bridging hydrogen is much less precisely known in I. The low-temperature X-ray derived distances for $HFe_4(CO)_{12}CH$ are Fe–H = 1.80 (4) Å, CH = 1.00 (4) Å, and FeC = 1.926 (5) Å, and it is clearly evident that the Fe–H–B (see above) interaction is much more symmetrical than the Fe–H–C interaction. This difference is consonant with a simple intuitive model consisting of a proton interacting with an Fe–C and Fe–B bond. Assuming the proton seeks out the position of maximum electron density for a given internuclear repulsion, then the less polar the bond the more symmetrical the Fe–H–X interaction should be.

Geometrical Structure in Terms of Electron Counting

Since the original suggestions by Wade and Mingos[17,18] that certain transition-metal cluster structures can be rationalized on the basis of assigned numbers of cluster bonding pairs, new cluster structures have served to both extend and delineate the limits of these electron-counting rules. The new ferraborane cluster, I, provides an interesting exercise in electron counting because of an apparent ambiguity in the number of cluster bonding pairs to be associated with this molecule.

Using Wade's rules at face value,[19] I can be considered a six skeletal pair (two electrons for each $Fe(CO)_3$ fragment, one for the Fe–H–Fe bridge H, and three for the BH_2 fragment) cluster with five cluster atoms. Thus, the structure is closo, and the five cluster atoms should lie at the vertices of a trigonal bipyramid (Figure Ib). If, on the other hand, all three hydrogens are considered to be endo and the boron interstitial, I has seven skeletal pairs (two electrons for each $Fe(CO)_3$, one for each H, and three for B) and four skeletal cluster atoms. Hence, the structure is arachno and the four cluster atoms should lie at four vertices of an octahedron (Figure 1b). In a strictly formal sense, either view is correct. Alternatively, one could focus on the requirements of the metals for 18 electrons as done by Mingos[18] and later Lauher.[20] In these terms I would be considered a 62-electron (14 from each $Fe(CO)_3$, five from BH_2, and one from H) saturated cluster that is analogous to the arachno description above. The closo description above would be analogous to a 60-electron unsaturated cluster and would require BH_2 to be a three-electron donor.

Ambiguities in the electron-counting procedures can disappear when one considers actual structural details. For butterfly systems, Bradley et al. have made the definite comparison in $Fe_4(CO)_{13}C$ and $Fe_4(CO)_{12}C{\cdot}CO_2CH_3^-$.[3] The former is considered to be a seven-pair arachno four-atom cluster with interstitial carbon (62-electron saturated cluster) whereas the latter is considered to be a six-pair closo five-atom cluster (60-electron unsaturated cluster). The former has a butterfly dihedral angle (θ) of 101° and a Fe–C–Fe (α) angle of 175° whereas for the latter the same angles are 130° and 148°. In addition the average Fe–Fe distance is considerably shorter (0.16 Å) in the latter (unsaturated) compound than in the former (saturated compound). As in an ideal seven-pair arachno four-atom homonuclear cluster the dihedral angle is 109° while it is 140° in a six-pair closo five-atom cluster (Figure 1), it is clear that the wing-tip bridging carbon in $Fe_4(CO)_{13}C$ is properly considered interstitial while in $Fe_4(CO)_{12}C{\cdot}CO_2CH_3^-$ it is not. The important qualitative point is that the effective number of cluster bonding electrons contributed by X is reflected in cluster structure. Similar parameters for I (dihedral angle 114°, Fe–B–Fe angle 162°, Fe–Fe distances marginally larger than in $Fe_4(CO)_{13}C$) favor the view of I as a seven-pair arachno four-atom cluster with an interstitial boron but, unfortunately, they are not definitive. For this reason, we have examined $HFe_4(CO)_{12}X$, X = BH_2, BH^-, and CH_2^+, by using the non-

(15) Haller, K. J.; Anderson, E. L.; Fehlner, T. P. *Inorg. Chem.* **1981**, *20*, 309. Anderson, E. L.; DeKock, R. L.; Fehlner, T. P. *Ibid.* **1981**, *20*, 3291.

(16) Fehlner, T. P.; Ragaini, J.; Mangion, M.; Shore, S. G. *J. Am. Chem. Soc.* **1976**, *98*, 7085. *Mangion*, M. M.; Ragaini, J. D.; Schmitkons, T. A.; Shore, S. C. *Ibid.* **1979**, *101*, 754.

(17) Wade, K. *J. Chem. Soc., Chem. Commun.* **1971**, 792. Wade, K. "Electron Deficient Compounds"; Nelson: London, 1971.

(18) Mingos, D. M. P. *Nature (London) Phys. Sci.* **1972**, *236*, 99.

(19) Wade, K. *Adv. Inorg. Chem. Radiochem.* **1976**, *18*, 1.

(20) Lauher, J. W. *J. Am. Chem. Soc.* **1978**, *100*, 5305.

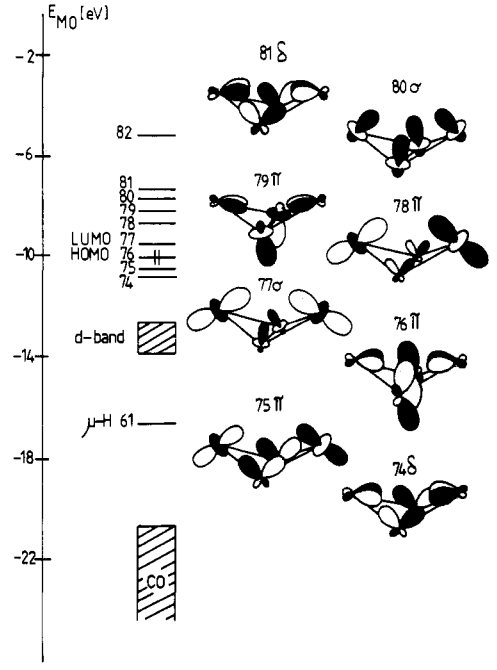

Figure 4. Schematic representation of the frontier MO's of the tetrairon butterfly fragment $HFe_4(CO)_{12}^+$.

parameterized Fenske–Hall quantum chemical technique in order to explore the relationship of I with known carbido clusters as well as to define more carefully the bonding capabilities of the tetrairon butterfly cluster.

Electronic Structure

The partitioning of a complex molecule into two closed-shell fragments is an effective way of delineating important features of electronic structure.[21] In the field of organometallic chemistry, the work of Hoffmann is the exemplar of this approach.[22] The Fenske–Hall technique[9] is particularly well designed for such an analysis as, after SCF convergence in the atomic basis set, the results may be transformed into a basis set of the fragment orbitals. Recent work by Fenske is illustrative in this regard.[23] A change of basis set is useful for large fragments, such as encountered in this work, as the correlation between fragment and complete molecule can be complex and difficult to construct otherwise. As the bonding capabilities of a metal butterfly fragment as found in I are of general interest and, to our knowledge, have not been examined in detail, we first discuss the frontier orbital characteristics of the $HFe_4(CO)_{12}^+$ fragment in the butterfly configuration indicated in Figure 1a.

Using the same symmetrized geometry as found in I, a Fenske–Hall calculation was performed on the tetrairon fragment $HFe_4(CO)_{12}^+$. The results are outlined in Figure 4 where, on the basis of orbital energies, eight frontier orbitals (MO's 74–81), three of which are occupied, can be identified. It is interesting to note that there is a unique Fe–H–Fe bridge bonding MO (61) that lies 2.8 eV below the lowest Fe orbitals, so-called t_{2g} (3d) band, and 4.1 eV above the onset of the CO MO's. This lends support to Mingos' analysis of M–H–M bonding as consisting of fairly localized three-center interactions.[24] As it is the character of the frontier orbitals that governs interactions with a ligand, an analysis of these in terms of bonding a bridging ligand (X in Figure 1a) is appropriate. It is convenient to classify these fragment orbitals both according to their symmetry with respect to the z (C_2) axis as given in Figure 5 and their metal–metal bonding character. This is done in Table V where the percentage of wing and hinge iron character is given as well. There are two frontier orbitals of σ symmetry, four of π symmetry, and two of δ symmetry. Of the four π orbitals, two have a nodal yz plane and are designated π_y, while two are labelled π_x having a nodal xz plane (Figure 4). Note particularly that MO 77 is given a σ symmetry label because of the predominent wing-tip character but that if the butterfly were flattened, it would have δ symmetry with respect to an incoming ligand. As is pointed out below, this MO is very important in determining the extent of perturbation of the ligand X caused by bonding to the butterfly. The symmetry analysis allows one to immediately predict that the δ symmetry orbitals (74 and 81) will not be important in considering the interaction of a simple ligand such as BH_2^- with the $HFe_4(CO)_{12}^+$ butterfly.

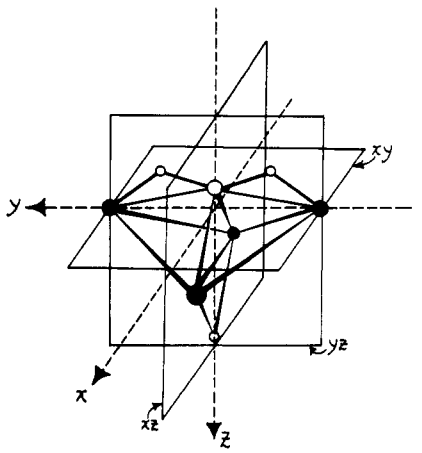

Figure 5. The master coordinate system used in all calculations.

Table V. Frontier MO's of the $HFe_4(CO)_{12}^+$ Fragment

MO	sym-metry[a]	% hinge iron	% wing iron	WH[b]	HH[b]
81	δ	47	34	ab	ab
80	σ	29	30	b	b
79	π_x	55	25	ab	ab
78	π_y	15	61	n	b
77 (LUMO)	σ	12	64	b	b
76 (HOMO)	π_x	47	32	b	ab
75	π_y	32	35	b	b
74	δ	34	45	b	ab

[a] With respect to C_2 axis. [b] b ≡ iron–iron bonding; ab ≡ iron–iron antibonding; W ≡ wing; H ≡ hinge.

$HFe_4(CO)_{12}BH_2$. A correlation diagram showing the formation of $HFe_4(CO)_{12}BH_2$ from the $HFe_4(CO)_{12}^+$ and BH_2^- fragments is given in Figure 6. As expected the major iron–borane interaction orbitals of the molecules are derived from the 2σ orbital of BH_2^- interacting with the σ orbitals of $HFe_4(CO)_{12}^+$ (77 and 80) and the 1π and 2π orbitals of BH_2^- interacting with the π orbitals of $HFe_4(CO)_{12}^+$ (76 and 78). The δ symmetry orbitals of the metal fragment do not participate in bonding; however, one remains filled and constitutes the HOMO of the molecule. To avoid as much confustion as possible, the term "MO" will be used henceforth only in reference to the complete molecule while "orbital" will be used when referring to the fragments. There are some unexpected features of the

(21) Burdett, J. K. "Molecular Shapes. Theoretical Models of Inorganic Stereochemistry"; Wiley: Sons: New York, 1980.
(22) Hoffmann, R. *Science (Washington, D.C.)* **1981**, *211*, 995.
(23) Kostic, N. M.; Fenske, R. F. *Organometallics* **1982**, *1*, 974.
(24) Mingos, D. M. P. *Pure Appl. Chem.* **1980**, *52*, 705.

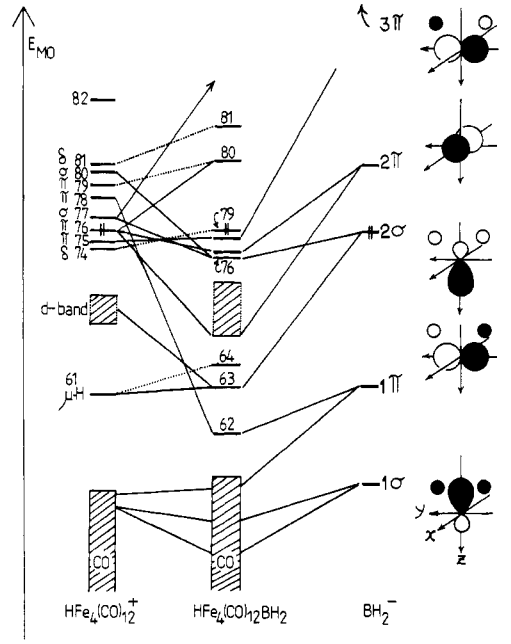

Figure 6. Fragment MO correlation diagram for the formation of $HFe_4(CO)_{12}BH_2$ from BH_2^- and $HFe_4(CO)_{12}^+$. The energy scales of the fragments have been shifted an arbitrary amount to match the HOMO's for convenience in viewing.

Table VI. Principal Metal-Ligand Bonding MO's in $HFe_4(CO)_{12}BH_2$ as % of Fragment Orbitals[a]

MO	E_{MO}, eV	% $HFe_4(CO)_{12}^+$ and symmetry type[b]	% BH_2^- and symmetry
78	−7.08	87% 75 (π), 5% 67 (M)	5% 3π, 1% 1π
77	−7.71	51% 76 (π), 10% 72 (M), 10% 70 (M), 13% 65 (M)	13% 2π
76	−7.88	20% 80 (σ), 20% 77 (σ), 20% 64 (M), 20% 62 (M)	15% 2σ
65	−11.04	8% 76 (π), 58% 65 (M)	25% 2π
63	−13.15	11% 64 (M), 24% 62 (M), 16% 61 (μH)	36% 2σ
62	−15.05	14% 78 (π)	64% 1π
59	−16.86	76% 58 (CO), 4% 55 (C)	8% 1σ
56	−17.35	63% 56 (CO)	8% 1π
53	−18.43	63% 50 (CO), 10% 58 (CO)	19% 1σ
49	−19.82	26% 50 (CO)	54% 1σ

[a] Only those with ≥3% contribution from BH_2^- included. [b] (M) = metal fragment d-band MO; (μM) = hinge Fe-H-Fe character; (CO) = carbonyl character.

bonding. One π symmetry, MM antibonding orbital (79) of the metal fragment does not interact with BH_2^- and becomes the LUMO of the molecule. The other strictly MM antibonding orbital of $HFe_4(CO)_{12}^+$ also remains empty in the complete molecule. The π symmetry orbital (75) interacts to a surprising extent with the high-lying empty 3π orbital of BH_2^-. The last observation has important qualitative implications.

From Table VI, it can be seen that there are ten principal cluster MO's of I involved in binding the BH_2^- moeity to the tetrairon fragment. Classifying the character of these MO's with respect to the BH_2 ligand, we find three of 1σ character, two of 2σ, two of 1 π, two of 2π, and one of 3π. Many of these orbitals have large contributions from the fragment "d band" orbitals, which, for clarity, are not shown in the correlation diagram (Figure 6). Yet an analysis of the net fragment–fragment overlap populations (Table VII) demonstrates that only four or perhaps five of these MO's can be considered principal BH_2–$HFe_4(CO)_{12}$ bonding MO's. They are MO's 62 (1π), 65 (2π), 76 (2σ), 77 (2π), and 78 (1π and 3π). Although the 1σ orbital

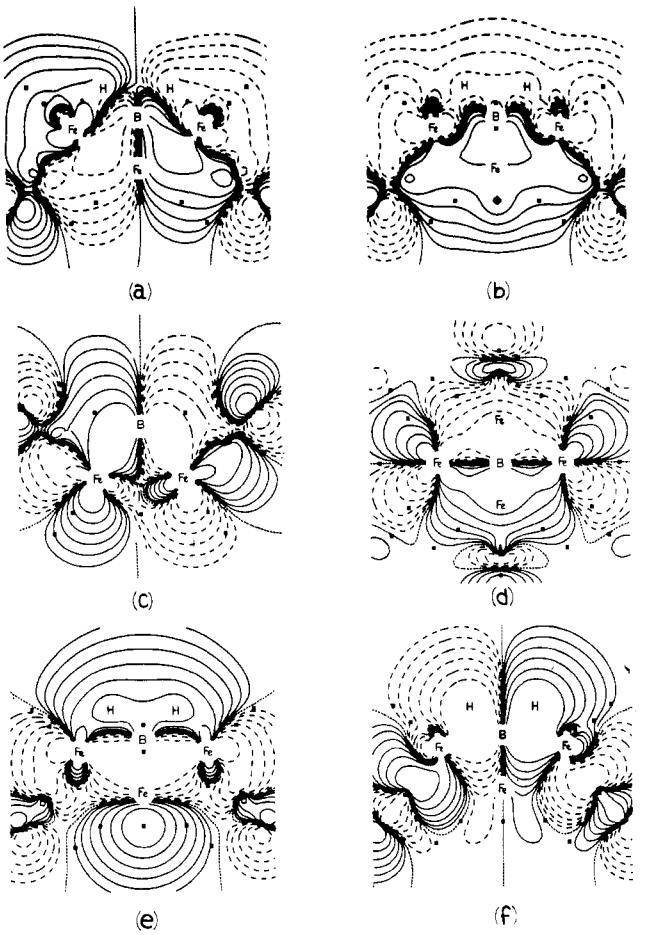

Figure 7. Amplitude contour diagrams for MO's (a) 78, (b) 76, (c) and (d) 65, (e) 63, and (f) 62 of $HFe_4(CO)_{12}BH_2$ exemplifying the principal modes of interaction between the fragments BH_2^- and $HFe_4(CO)_{12}^+$. The contours are for the *yz* plane as defined in Figure 5 except for (c) and (d) which are of the *xz* and xy planes, respectively. Skeletal atoms in the plane are denoted by symbol, whereas the positions of the other atoms when projected onto the plane of the contour diagram are denoted by asterisks. Each diagram contains six contours, each succeeding contour differing from the previous one by a factor of 2. The value of the largest contour for each diagram is 0.05 electron au^{-3}.

of BH_2^- and the d-band orbitals (62, 65, 67) of $HFe_4(CO)_{12}^+$ are well represented in Table VI, they do not contribute extensively to the overlap populations. A more detailed discussion of the important borane–metal bonding MO's (62, 65, 76, 77, and 78) follows.

2σ Character. Figure 6 and Table VI delineate the participation of the tetrairon fragment orbitals 62, 64, 77, and 80 in MO's of I containing BH_2 2σ character. The fragment–fragment overlap populations demonstrate that the two empty, acceptor orbitals 77 and 80 are the important ones as far as the bonding interactions are concerned. An amplitude contour diagram of MO 76 of **I** is shown in Figure 7b and demonstrates the cluster bonding nature of the 2σ interaction. It is important to note that while fragment orbital 80 has about equivalent wing-tip and hinge contributions of the same sign (Figure 4) fragment orbital 77 has predominantly wing-tip character, with wing-tip and hinge contributions of different sign. Thus, when the BH_2^- fragment is placed deeply in the butterfly as found in I, the interactions of the 2σ orbital with 77 are all bonding whereas those with 80 are bonding and antibonding. In both cases the net interaction is bonding (Table VII). Note that if the BH_2 ligand were rotated through 90°, the favorable interaction with 77 would be

Table VII. Fragment Mulliken Overlap Populations[a] of $HFe_4(CO)_{12}^+$ and BH_2^- in $HFe_4(CO)_{12}BH_2$

MO in $HFe_4(CO)_{12}^+$ fragment	MO's in BH_2^- ligand					
	1σ	1π	2σ	2π	3π	3σ
80 (σ)	(−0.099)		0.150 (0.138)			
78 (π)		0.213 (0.184)				
77 (σ)	0.032		0.162 (0.112)			
76 (π)				0.240 (0.213)		
75 (π)					0.093 (0.063)	
67 (M)					0.029	
65 (M)				0.031 (0.025)		
62 (M)			0.037 (0.032)			
50 (CO)	−0.033					
49 (CO)		−0.047 (−0.023)				

[a] Overlap ≥ 0.02 only included. Numbers in parentheses refer to $HFe_4(CO)_{12}(CH_2)^+$.

lost and could not be compensated for by the ligand 2σ orbital interacting with any other fragment orbital. The (77-2σ) interaction is clearly one of the interactions that is important in explaining the observed orientation of the BH_2 ligand with respect to the iron butterfly.

Although the d-band orbitals of the tetrairon fragment 62 and 64 contribute substantially to MO 76 of I, they only provide a modest contribution to the net overlap populations (Table VII). Likewise even though MO 63 of I contains 36% 2σ BH_2^- character, the associated net overlap is not significant. This is not obvious from looking at the amplitude contour diagram for MO 63 of I (Figure 7) and suggests some caution in relying on orbital contours exclusively in discussing metal–ligand bonding.

2π Character. The 2π BH_2^- orbital has no hydrogen character; it has pure p_x character directed along an axis parallel to the Fe–Fe hinge bond in the known structure of I. The wing-tip irons therefore lie in a nodal plane with respect to the ligand. The tetrairon fragment orbitals 76 and 79 have the correct symmetry for interaction with the 2π ligand orbital (Figure 4), but only 76 has a significant interaction as judged by the overlap populations (Table VII). As already noted the fragment orbital 79 is unaffected by the ligand and becomes the LUMO of I. The reason for this is that orbital 79 has 55% hinge character (Table V) and the hinge lobes point away from a potential ligand (Figure 4). For compound I, the 2π character is distributed between MO's 65 and 77 both of which also contain significant percentages of fragment orbital 76. Amplitude contour plots of MO 65 and 77 of I are similar, and two cuts of MO 65 are shown in Figure 7c,d. Figure 7c shows a cut through the xz plane (Figure 5) of I containing the hinge iron and boron atoms. The good overlap of the hinge atom hybrids with the boron 2p function is evident. Figure 7d shows the xy plane containing the wing-tip iron and demonstrates cluster bonding in this plane as well.

1π and 3π Character. The 1π and 3π orbitals of BH_2^- differ in that the former is BH bonding while the latter is BH antibonding. With respect to interactions with $HFe_4(CO)_{12}^+$ they are similar; however, one would ordinarily ignore the 3π orbital because it lies at such high energy. Yet it is clear from Table VII that both the 1π and 3π orbitals of BH_2^- are important in the net interaction with the tetrairon fragment. The orbitals of the tetrairon fragment that interact strongly with these ligand orbitals are 78 (with 1π) and 75 (with 3π). As shown in Figure 4, orbital 78 that is empty in the fragment is well set up to interact with the 1π orbital of BH_2^-. A contour diagram of the resulting cluster MO of I (62, Table VI) is shown in Figure 7f. This MO is clearly hinge-wing boron bonding with an xz nodal plane but is Fe(wing)–H–B bonding as well. The large wing-tip character of the fragment orbital (Table V) enhances this aspect of the bonding. As also shown in Figure 4, orbital 75, which is filled in the tetrairon fragment, is beautifully set up to interact with the empty 3π, not only with the boron $2p_y$ component but also with the hydrogen 1s. Thus, the resulting MO in I is boron–iron bonding and BH antibonding but also H–Fe(wing-tip) bonding. Clearly both orbitals 75 and 78 of the tetrairon fragment are important in determining both the orientation of the BH_2^- ligand as well as the location of the boron within the butterfly. Perhaps more important is the fact that to the extent to which that the 3π is populated in bonding BH_2^- to the tetrairon fragment (0.19 e) the BH bond will be weakened. Clearly the BH_2^- ligand is significantly perturbed on being bound to the iron butterfly.

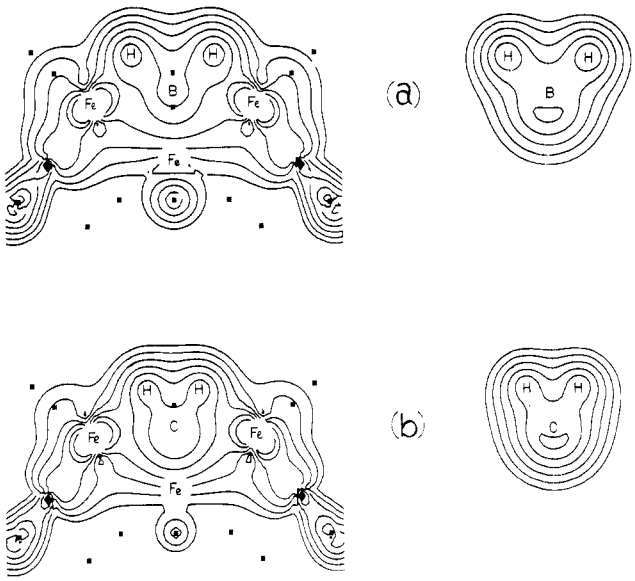

Figure 8. Contour density diagrams for the principal metal–ligand bonding MO's for (a) $HFe_4(CO)_{12}BH_2$ and (b) $HFe_4(CO)_{12}CH_2^+$ and all filled MO's of (a) BH_2^- and (b) CH_2 ligands. The diagram for $HFe_4(CO)_{12}BH_2$ results from MO's that contain 85% of BH_2 AO character while the diagram for $HFe_4(CO)_{12}CH_2^+$ with the density for the analogous orbitals contains 94% of the CH_2 AO character. Adding five more MO's to the density diagram for $HFe_4(CO)_{12}BH_2$ did not change the qualitative observations described in the text. These diagrams for the complexes are all in the yz plane (Figure 5) containing wing-tip iron atoms, XH_2 unit, and bridging-hinge H atom. Other atoms are projected on the yz plane and are indicated by asterisks. Each diagram is represented by six contours, each succeeding contour differing from the last by a factor of 2. The values of the largest contour (units of electrons au^{-3}) are 0.15 for the complexes and 0.3 for the free ligands.

Electron Densities. The electron density distribution represented by the principal metal–ligand bonding MO's given in Table VI is presented in a contour diagram in Figure 8a. The figure also shows a density contour diagram for all the filled orbitals of free BH_2^- with the same geometry as the bound ligand. Comparison of the density diagrams for free and bound ligands shows considerable redistribution of electronic charge associated with BH_2^- upon being bound to the tetrairon fragment. The most obvious difference is the change in the bonding of the H's from two-center BH interactions to three-center BHFe

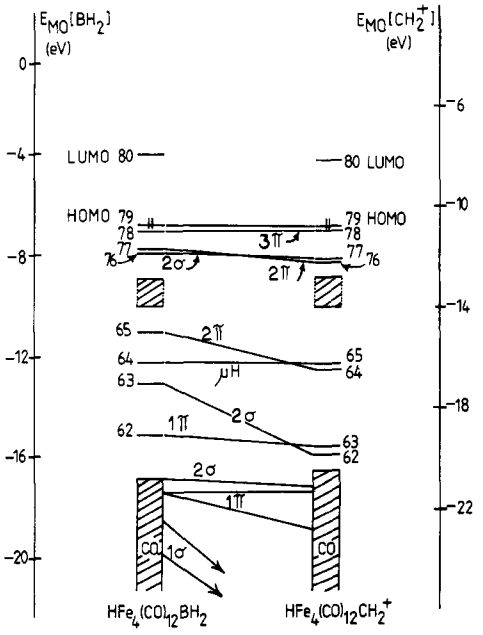

Figure 9. Correlation of the MO's of $HFe_4(CO)_{12}BH_2$ and $HFe_4(CO)_{12}CH_2^+$. The energy scale of the cation is increased by ~4 eV to match the HOMO's for convenience.

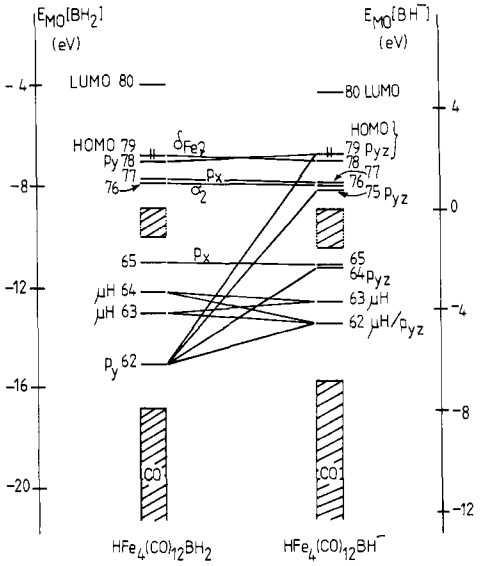

Figure 10. Correlation of the MO's for $HFe_4(CO)_{12}BH_2$ and $HFe_4(CO)_{12}BH^-$. The energy scale for the anion has been shifted ~4 eV to lower energy to match the HOMO's for convenience.

interactions. Clearly the BH_2^- ligand has been partially disassembled, and the H's in I are involved in direct skeletal bonding. The source of the perturbation lies in the mixing of the empty 3π BH_2^- with the filled orbital 75 of $HFe_4(CO)_{12}^+$. As the 3π is BH antibonding there is an effective transfer of charge from between the BH nuclei to the hydrogens and to the skeleton. We suggest that the ability of the tetrairon cluster to interact effectively with an empty ligand X–H antibonding orbital is a property to be associated with this array of metal atoms whether it be on a discrete cluster or on a metal surface.[25]

For comparative purposes, we have carried out calculations on $HFe_4(CO)_{12}CH_2^+$. Shriver et al.[2] have shown that a compound with the formula $Fe_4(CO)_{12}CH_3^+$ is an intermediate in the conversion of $Fe_4(CO)_{13}^{2-}$ to CH_4 and other products. The originally postulated structure, $HFe_4(CO)_{12}CH_2^+$, is analogous to that found for isoelectronic I; however, recent NMR studies indicate a more proper formulation is $H_2Fe_4(CO)_{12}CH^+$.[26] Despite not being the most stable structure, fragment analysis of $HFe_4(CO)_{12}CH_2^+$ indicates that CH_2 interacts with the tetrairon fragment in qualitatively the same manner as BH_2^-. Figure 9 summarizes the main differences between the two complexes in terms of MO energy changes all of which are reasonable in terms of substituting C for B. Amplitude contour plots confirm the similarities. Figure 8b illustrates the electron distributions for the free CH_2 ligand as well as the principal metal–ligand bonding orbitals analogous to those for I. In this comparison, it is obvious that CH_2 retains a major portion of its ligand character upon being bound to the tetrairon fragment. In addition this comparison confirms the significance of the electron density changes observed for I and free BH_2^-.

The source of the difference between I and $HFe_4(CO)_{12}CH_2^+$ is revealed in Table VII where the overlap populations between the $HFe_4(CO)_{12}^+$ fragment and the two ligands are compared. Note that the net interaction of the 3π ligand orbital for CH_2 is only half that for BH_2^- (the Mulliken population of the 3π orbital is 0.14 e in the CH_2 derivative). This means that there is less CH antibonding character mixed in on CH_2 binding than upon BH_2^- binding to the tetrairon fragment. This is pleasing as we have previously suggested metalloboranes as valid models for high-energy states of metal-bound hydrocarbon fragments.[27] Thus, we now suggest that CH bond breaking takes place by the donation of electron density from the metal cluster to an empty CH antibonding MO. Further, this process is facilitated by the tetrairon butterfly cluster and would not be possible in a mononuclear complex.[28] The fact that the observed site of protonation is on a FeFe bond rather than a FeC bond in $HFe(CO)_{12}CH$ may be associated with the required small HCH angle (66°) for a structure analogous to I.

Deprotonation of $HFe_4(CO)_{12}BH_2$. Deprotonation of I to yield $HFe_4(CO)_{12}BH^-$ is possible,[29] and a fragment analysis based on the results of a Fenske-Hall calculation shows some interesting features. First, there is considerable increase in the mixing of metal fragment MO's and BH^{2-} MO's upon formation of the complex compared to I. There are 12 complex MO's containing greater than 5% ligand character, viz., 10 MO's in I. A correlation between the MO's of I and $HFe_4(CO)_{12}BH^-$ (Figure 10) shows a striking change in MO 62 of I on deprotonation. This MO is not only greatly destabilized but has its character spread throughout four filled MO's (62, 64, 75, and 79) of HFe_4-

(25) For other theoretical results on surface M–H interactions see: Gavin, R. M., Jr.; Reutt, J.; Muetterties, E. L. *Proc. Natl. Acad. Sci. U.S.A.* **1981**, *78*, 3981.

(26) Drezdzon, M. A.; Whitmire, K. H.; Shriver, D. F. "Abstracts of Papers", 184th National Meeting of the American Chemical Society Kansas City, Sept 1982; American Chemical Society: Washington, D.C., 1982; INORG 176. See Scheme I in: Drezdon, M. A.; Whitmire, K. H.; Bhattacharyya, A. A.; Hsu, W.-L.; Nagel, C. C.; Shore, S. G.; Shriver, D. *J. Am. Chem. Soc.* **1982**, *104*, 5630.

(27) Housecroft, C. E.; Fehlner, T. P. *Adv. Organomet. Chem.* **1982**, *21*, 57. Gilbert, K. B.; Boocock, S. K.; Shore, S. G. In "Comprehensive Organometallic Chemistry"; Wilkinson, G., Stone, F. G. A., Abel, E. W., Eds.; Pergamon Press: New York, 1982; Vol. 6, p 879.

(28) There is an ongoing search to define the unique ways a metal cluster can interact with a ligand. We believe this to be one. For a general discussion see: Muetterties, E. L.; Rhodin, T. N.; Band, E.; Brucker, C. F.; Pretzer, W. R. *Chem. Rev.* **1979**, *79*, 91.

(29) Metalloboranes do undergo deprotonation reactions[16] but note that the proton was removed from the BHB bond in preference to the BHFe bond. In principle, one must also consider removal of the FeHFe proton; however, the calculated Mulliken charges of the bridging hydrogens (FeHB = 0.03–; FeHFe = 0.32–) suggest a considerably higher protonic character for the FeHB bridging hydrogen.

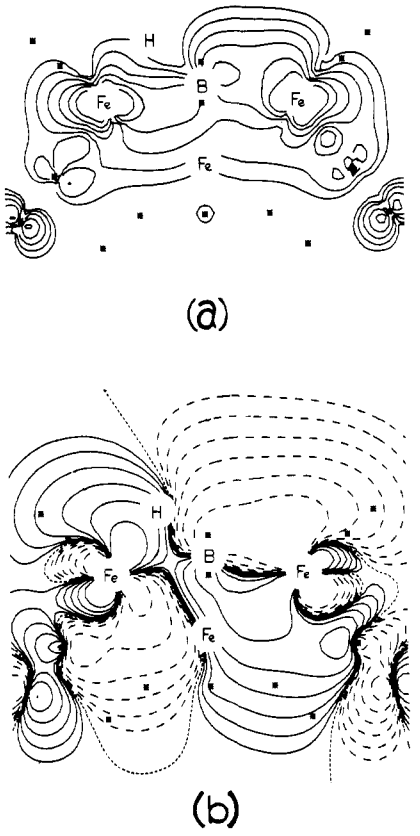

Figure 11. (a) Density contour diagram for the sum of MO's 62, 64, 75, and 79 for $HFe_4(CO)_{12}BH^-$ and (b) amplitude plot for MO 79 (the HOMO) of $HFe_4(CO)_{12}BH^-$. The contours are in the *yz* plane (Figure 5), and all atoms either in or projected onto this plane are indicated by symbols or asterisks. Each diagram is represented by six contours, each succeeding contour differing from the last by a factor of 2. The largest contour is (a) 0.15 and (b) 0.05 electrons au^{-3}.

$(CO)_{12}BH^-$. MO 62 of I is Fe(wing-tip)–B–H bonding (Figure 7), and it is not surprising that it is perturbed upon removing a proton. Amplitude plots of each of MO's 62, 64, 75, and 79 in $HFe_4(CO)_{12}BH^-$ have significant values in the region between the wing-tip iron and boron from where the proton was removed. This is clearly visible in the amplitude plot of MO 79 (exemplary of the four related Fe–B MO's) in Figure 11b. It is important to note that in contrast to I where the HOMO (79) is clearly located on the tetrairon fragment and is Fe-Fe bonding, here the HOMO is involved in B–Fe bonding, the Fe–Fe bonding MO becoming the second highest filled MO in $HFe_4(CO)_{12}BH^-$ (Figure 10). In Figure 11a a density plot of the four orbitals involving the Fe–B bond suggests a site of Lewis basicity on the $HFe_4(CO)_{12}BH^-$ complex associated with the Fe–B bond. There is now ample evidence to suggest that compounds containing such basic sites are likely candidates for cluster building reactions with electrophilic reagents.[27]

Although to our knowledge, $HFe_4(CO)_{12}BH^-$ has not yet been isolated, its hydrocarbon analogue $HFe_4(CO)_{12}CH$ has and, as noted above, full structural data are available.[1] Just as the tetrairon butterfly fragment possesses orbital properties that lead to BH bond weakening in I and in $HFe_4(CO)_{12}BH^-$, so too will the same metal fragment be responsible for CH bond weakening and subsequent activation in $HFe_4(CO)_{12}CH$. Such a phenomenon has important ramifications with respect to CH adsorption on metal surfaces. A detailed orbital analysis of $HFe_4(CO)_{12}CH$ is presented elsewhere.[30]

Acknowledgment. The support of the National Science Foundation under Grant CHE 81-09503 is gratefully acknowledged. We also thank the Notre Dame Computing Center for computing time and Prof. Roger DeKock for aid with the transformations.

Registry No. $HFe_4(CO)_{12}BH_2$, 80572-82-3.

Supplementary Material Available: A listing of observed and calculated structure factor amplitudes (11 pages). Ordering information is given on any current masthead page.

(30) Housecroft, C. E.; Fehlner, T. P. *Organometallics* **1983**, *2*, 690.